Phase Behavior and Crystallization Analysis in Binary Crystalline Blends of Syndiotactic Polypropylene and Ethylene—Propylene Random Copolymer

CHING-I HUANG,[1] CHUN-PIN CHANG,[2] KATSUMI SHIMIZU,[3]* CHARLES C. HAN[3†]

[1]National Taiwan University, Institute of Polymer Science and Engineering, Taipei 106, Taiwan

[2]National Taiwan University of Science and Technology, Institute of Materials Science and Technology, Taipei 106, Taiwan

[3]National Institute of Standards and Technology, Polymers Division, Gaithersburg, Maryland 20899

Received 7 November 2003; revised 7 April 2004; accepted 13 May 2004
DOI: 10.1002/polb.20188
Published online in Wiley InterScience (www.interscience.wiley.com).

ABSTRACT: The effects of liquid–liquid (L–L) phase separation on the crystallization behavior of binary syndiotactic polypropylene (sPP) and ethylene–propylene random copolymer (PEP) mixtures are examined by phase-contrast microscopy (PCM), differential scanning calorimetry (DSC), and cloud point measurements. The PCM experiments reveal that blends of sPP and PEP exhibit a lower critical solution temperature behavior in the melt. The L–L phase diagram, constructed in terms of temperature (T) and composition by cloud point measurements, follows the prediction of the Flory–Huggins theory with the interaction parameter between sPP and PEP [$\chi(T) = 0.01153 - 4.5738/T$ (K)]. When the blends are melted within the two liquid-phase (α and β) regions, because of the fact that each phase domain reaches the equilibrium concentration ϕ^{α}_{PEP} and ϕ^{β}_{PEP} as well as the phase volume fraction ν^{α} and ν^{β}, the crystallinity of each component obeys the equation $X_{C,I} = \nu^{\alpha} X^{\alpha}_{C,I} + \nu^{\beta} X^{\beta}_{C,I}$, I = PEP, sPP. Also, the equilibrium melting temperatures of both components remain constants, slightly lower than those of neat polymers. For the sPP/PEP blends crystallized from one homogeneous phase in the melt, we observe that the crystallizability of the major component is not greatly affected upon blending. However, the crystallization behavior of the minority component in the presence of the major component is strongly dependent on the crystallization temperature (T_c). When T_c is high, because the decreasing degree of the minority mobility is much greater than the increasing degree of the formed nuclei, the crystallizability of the minor component is depressed significantly. On the other hand, the promotion of the minority crystallizability in the intermediate regime of T_c is mainly because of the large increase of the heterogeneous nuclei upon blending with a major component. © 2004 Wiley Periodicals, Inc. J Polym Sci Part B: Polym Phys 42: 2995–3005, 2004

Keywords: blends; crystallization; spinodal decomposition; liquid–liquid phase separation

INTRODUCTION

Miscibility and crystallization in polymer blends continue to attract a lot of interest because they involve important issues concerning control of supermolecular structures as well as the corresponding physical and material properties. Although most of the research has focused on amorphous/crystalline polymer blends,[1–18] few conclusive studies on crystalline/crystalline polymer blends exist.[2,14,19–23] Because of the effects of liquid–liquid (L–L) separation associated with the crystallization of both components, phase behavior of binary crystalline blends becomes very complicated. Although there have been some studies that have focused on the effects of L–L separation on the resulting crys-

Correspondence to: C.-I Huang (E-mail: chingih@ntu.edu.tw
Present address: High-throughput Factory, Harima Institute, RIKEN, Hyogo 679–5418, Japan.
†*Present address:* Joint Laboratory of Polymer Science and Materials, Institute of Chemistry, Chinese Academy of Sciences, Beijing 100080, People's Republic of China.

Journal of Polymer Science: Part B: Polymer Physics, Vol. 42, 2995–3005 (2004)

tallization morphology, the phase behavior in both the liquid and solid state and the crystallization analysis of binary crystalline blends have not been fully explored. In this article, we systematically examine the phase behavior as well as the crystallization behavior of binary crystalline polymer blends. In particular, we construct the phase diagram and examine the effects of L–L phase separation on the crystallization behavior of both components.

We consider a binary crystalline blend of syndiotactic polypropylene (sPP) and propylene–ethylene random copolymer (PEP). The melting point of sPP is about 130 °C. The PEP contains 85–95 wt % crystallizable isotactic propylene (iPP) and has a melting temperature around 165 °C. Much of the related research has focused on crystalline iPP/amorphous PEP,[2–3,8–9,13–15,17] and crystalline sPP/crystalline iPP blends.[21–23] For crystalline iPP/amorphous PEP systems, most studies have been concerned with the effects of L–L separation on the crystallization morphology of blends as well as the melting point of iPP. It is well known that the blends exhibit lower critical solution temperature (LCST) phase behavior in the melt. Because of the rapid crystallization process of iPP, the liquid–liquid separation morphology that developed above the melting temperature of iPP can be locked into the crystallization morphology.[3] As for the effects of PEP addition on the melting temperature of iPP, Hashimoto et al.[3] observed the iPP melting-point depression by examining the iPP and PEP blends with weight ratios of 5/5 and 7/3, which they claimed results from a small amount of PEP dissolved in the iPP rich domains. Although D'Orazio et al.[8] examined the iPP/PEP blends with ratios of 9/1 and 8/2, they showed that the melting temperature of iPP is independent of blend concentration, indicating that iPP and PEP are highly incompatible in the molten state. Because both Hashimoto et al. and D'Orazio et al. studied the iPP/PEP blends within a very narrow region of polymer concentration, their results for the iPP melting point as a function of polymer concentration were also not conclusive. Therefore, the effects of blend concentration, associated with the immiscibility between both components in the melt, on the melting temperature behavior as well as the crystallinity of components in the mixtures must be further analyzed.

For crystalline sPP/crystalline iPP blends, a few studies exist on the effects of L–L separation on the crystallization morphology and the thermal crystallization behavior of both components.[21–23] For example, Kressler et al.[22] observed neither sPP nor iPP melting-point depressions, which indicates that sPP and iPP are completely immiscible in the melt. Phillips[23] concluded that iPP and sPP are immiscible in the melt by observing that the crystallization morphology depends on the annealing time above the melting temperature of both components. These studies were concerned with the crystallization morphology of binary crystalline sPP and iPP blends associated with the L–L separation in the melt; However, both the thermodynamic and kinetic phase behavior in the melt for sPP and iPP blends, and the effects of L–L separation on the melting behavior as well as the crystallinity of both crystalline components, have not yet been fully examined.

We examine a series of binary crystalline sPP/PEP blends with weight fractions of PEP (wt_{PEP}) varying from 0 to 1. We study the spinodal decomposition kinetics in the liquid state by phase-contrast microscopy. We determine the L–L phase boundary by cloud point measurements. By comparing the measured L–L coexistence curve with the theoretical prediction based on the Flory–Huggins formalism, we quantify the immiscibility parameter between sPP and PEP as a function of temperature. With the aid of differential scanning calorimetry (DSC) experiments, we analyze the melting temperature and the crystallinity of both components as a function of blend concentration and crystallization temperature. In a combination of the crystallinity analysis from DSC and the L–L segregation analysis from the LCST coexistence curve, the effects of L–L phase separation on the crystallization behavior are quantified. It should be noted that with the DSC analysis in our study, associated with thermodynamic analysis, we are the first researchers to quantitatively determine the crystallinity contributed from each crystalline component as well as from each phase-separated domain.

EXPERIMENTAL

Materials and Sample Preparation

The materials used in this study were mixtures of syndiotactic polypropylene (sPP) with a weight-average molecular weight (M_w) = 127,000 and a number-average molecular weight (M_n) = 54,000, and random PEP with 5–15 wt % ethylene. Both materials were purchased from Aldrich Chemical Company. The melting temperature of sPP and

PEP is around 130 and 165 °C, respectively. The blends were prepared by dissolving different weight fractions of PEP in hot *p*-xylene at a temperature around 110 °C. The solutions were precipitated into a large amount of methanol cooled with ice. These precipitates were then filtered and dried *in vacuo* at 70 °C for 12 h to ensure that the solvent was completely removed.

Phase-Contrast Microscopy (PCM)

The structure evolution in the melt was observed in real time by phase-contrast microscopy. The samples were first hot-pressed between two glass plates at 130–140 °C to form thin films of about 25 μm in thickness. The film specimens were then heated to the desired demixing temperature (T_d), above the melting temperatures of both sPP and PEP, when the time evolution of the resulting decomposition patterns was recorded by a Sony CCD video camera.

Cloud Point Measurement

A cloud point measurement, using light scattering, was performed with a He–Ne laser of wavelength λ = 632.8 nm at a given scattering angle θ = 25°. The samples were first hot-pressed between two glass plates at 130–140 °C to form films of about 0.5 mm in thickness. The films were then heated on a Linkam THMS600 hot stage at various heating rates, and the scattered intensities were measured to determine the liquid–liquid phase boundary.

DSC

The thermal crystallization behavior of sPP/PEP blends was analyzed by a PerkinElmer DSC-7 differential scanning calorimeter. First, the samples were heated from room temperature to 200 °C and annealed for 10 min in the melt. The samples were then quickly quenched to the desired crystallization temperature (T_c) at a cooling rate of 130 °C/min. After complete crystallization, the samples were reheated to a melt with a heating rate of 4 °C/min. The heat flow per gram of the sample evolved during the scanning process was measured as a function of temperature, from which the melting temperatures of both sPP and PEP components were determined from the maxima of the melting peaks, and the apparent enthalpy of melting per gram (ΔH^*_{blend}) was obtained from the areas of the melting peaks. With a further detailed analysis of ΔH^*_{blend}, as shown in the Results and Discussion section, the enthalpy contribution from sPP and PEP, respectively, was separated. Hence, the crystallinity of each component was determined.

RESULTS AND DISCUSSION

Phase Behavior in the Liquid State

Figure 1 displays the time evolution of morphology under phase-contrast microscopy for the sPP/PEP blend with a weight fraction of PEP (wt_{PEP} = 0.5), demixed at T_d = 180 °C, 200 °C, and 220 °C, respectively. As can be clearly seen, the modulated interconnected structures that are characteristic of L–L spinodal decomposition develop and coarsen with time. Also, the time-resolved phase-separated domain size increases with the T_d. This indicates that the sPP and PEP blends have a LCST phase behavior.

Figure 2(a) shows the variation of the scattered intensity for sPP/PEP blends with wt_{PEP} varying from 0.1 to 0.9 at a heating rate of 1 °C/min. During the heating run, the scattered intensity for the blends remains somewhat constant and then decays gradually, indicating the melting of PEP crystals associated with the homogenization of PEP and sPP chains in the blends. With further heating, we observe that the scattered intensity for systems with $wt_{PEP} \geq 0.3$ begins to increase. This is because the immiscibility between sPP and PEP is significant enough for the blends to undergo L–L phase separation. Figure 2(b) plots the temperature when the intensity begins to increase, which is defined as L-L phase separation temperature (T_{ps}), versus heating rate for various values of wt_{PEP}. The L–L phase coexistence temperature was then determined by extrapolating T_{ps} to a zero heating rate.

To describe this L–L phase behavior for sPP/PEP blends, we construct the thermodynamics with the Flory–Huggins mean-field theory.[24] The free energy of mixing per lattice site is therefore give by

$$\Delta g = k_B T\left(\frac{\phi_{PEP}}{N_{PEP,w}} \ln \phi_{PEP} + \frac{\phi_{sPP}}{N_{sPP,w}} \ln \phi_{sPP} + \chi\phi_{PEP}\phi_{sPP}\right) \quad (1)$$

where χ is the Flory interaction parameter between sPP and PEP, $N_{PEP,w}$ and $N_{sPP,w}$ are the weight-average degrees of polymerization, and

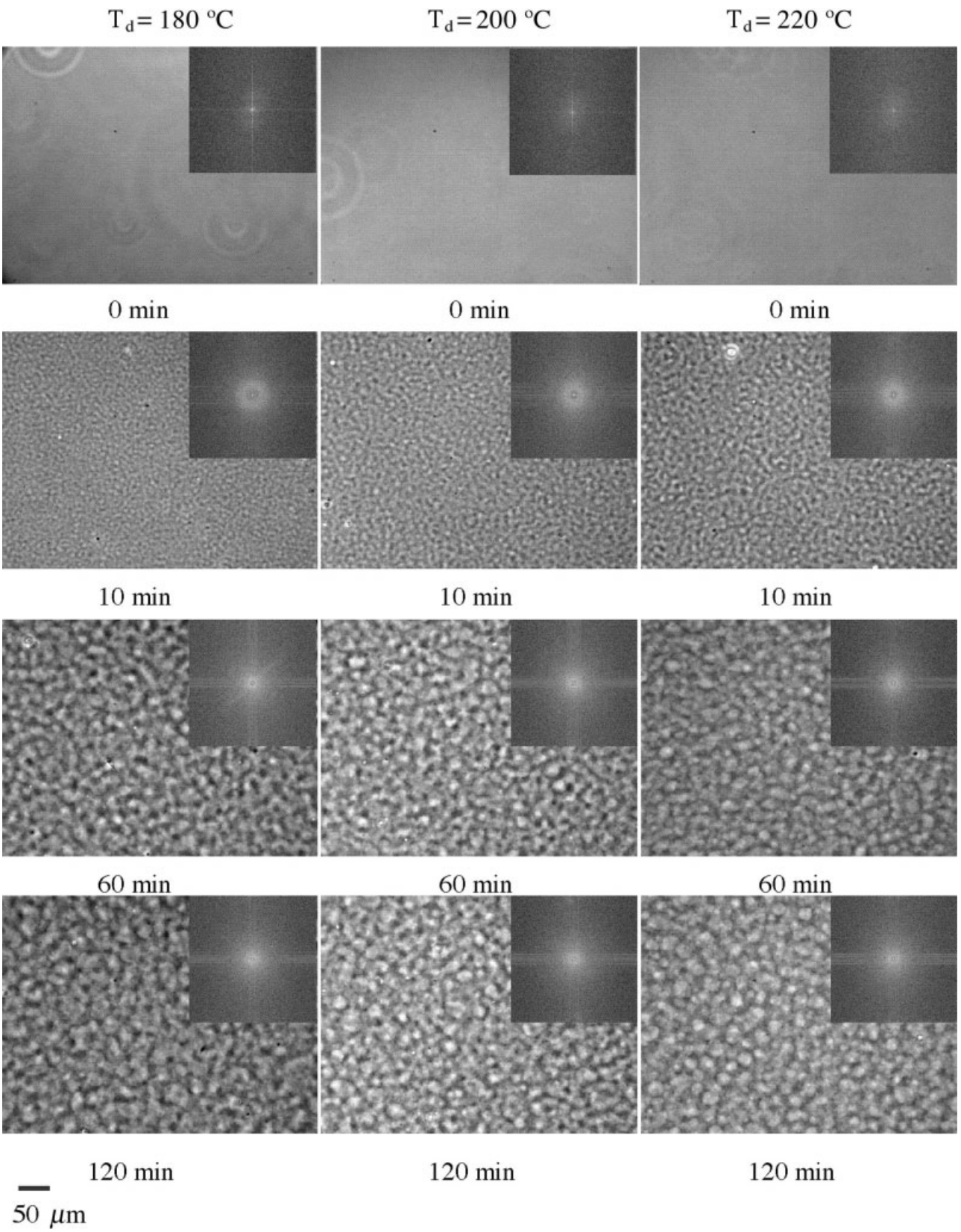

Figure 1. Time evolution of phase-contrast micrographs for the sPP/PEP blend with wt_{PEP} = 0.5 demixed at T_d = 180 °C, 200 °C, and 220 °C, respectively. The scale bar represents 50 μm.

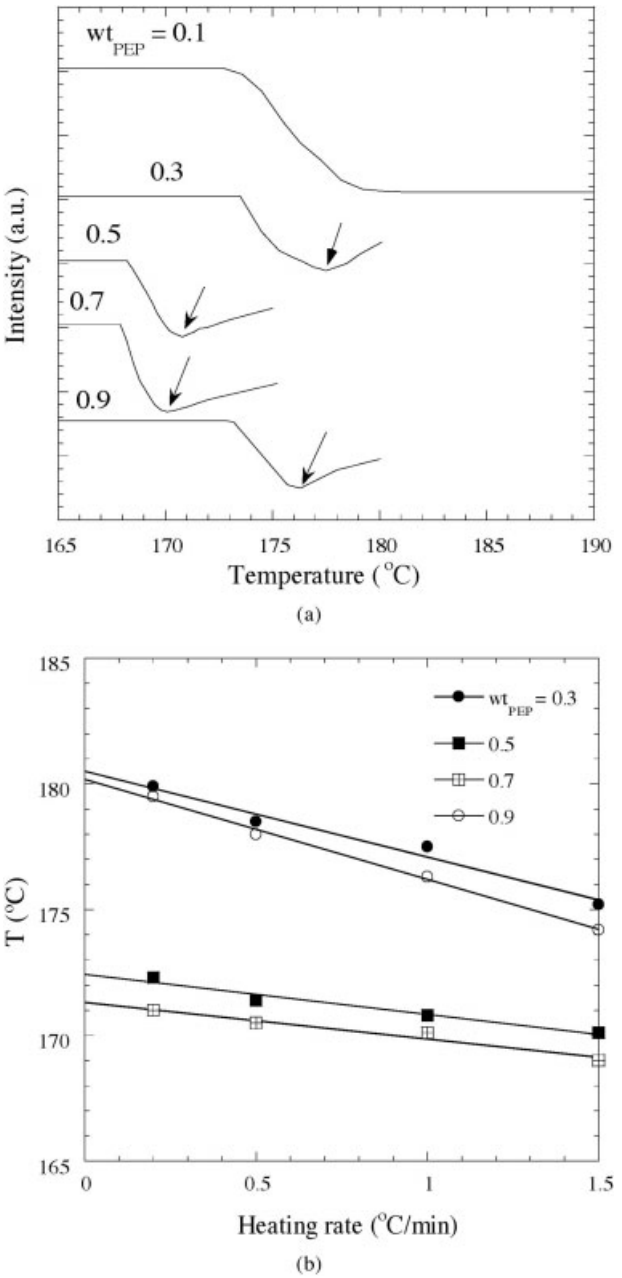

Figure 2. (a) Variation of the scattered intensity at a given scattering angle (θ= 25°) for the sPP/PEP blends with various values of wt_{PEP} at a heating rate of 1 °C/min. (b) Plot of the L–L phase separation temperature (T_{ps}) the heating rate for blends with various values of wt_{PEP}.

ϕ_{PEP} and ϕ_{sPP} are the average volume fractions of PEP and sPP, respectively. We assume that the system is incompressible both locally and globally, and that each monomer type has the same statistical segment length. For simplicity, both polydisperse PEP and sPP are characterized as monodisperse components with degrees of polymerization equal to $N_{PEP,w}$ and $N_{sPP,w}$, respectively. For a given set of parameters $N_{PEP,w}$ and $N_{sPP,w}$, the corresponding phase diagram, in terms of χ and ϕ_{PEP}, is calculated by equating the chemical potential of each component in the coexisting phases. The chemical potentials of PEP and sPP have the form

$$\mu_{PEP} = RT\left(\ln \phi_{PEP} + \phi_{sPP}\left(1 - \frac{N_{PEP,w}}{N_{sPP,w}}\right) + \chi N_{PEP,w}\phi_{sPP}^2\right)$$

$$\mu_{sPP} = RT\left(\ln \phi_{sPP} + \phi_{PEP}\left(1 - \frac{N_{sPP,w}}{N_{PEP,w}}\right) + \chi N_{sPP,w}\phi_{PEP}^2\right) \quad (2)$$

In our systems, $M_{sPP,w}$ = 127,000 and thus $N_{sPP,w}$ is equal to 3024. Although $M_{PEP,w}$ is not provided, we can calculate the binodal curves for a given parameter $N_{PEP,w}$, and compare them with the L–L coexistence temperatures obtained from various experiments. We find that both theoretical and experimental results are in excellent agreement when $N_{PEP,w}$ = 1008. Therefore, we select the calculated binodal curves for $N_{PEP,w}$ = 1008 as the best fit to describe the LCST phase behavior for sPP/PEP blends, as shown in Figure 3, where we plot the corresponding calculated phase diagram in terms of χ and wt_{PEP}. Note that because the mass densities of amorphous PEP and sPP are equal to 0.852 and 0.856 g/cm^3, respectively,[25] both values of ϕ_{PEP} and wt_{PEP} are almost identical. By fitting the cloud point temperatures from experiments with the calculated values of the interaction parameter χ in the coexistence curve in Figure 3, we obtain χ as a function of temperature in units of K as $\chi(T)$ = 0.01153 − 4.5738/T. In Figure 3, we also include the equilibrium melting temperatures $T^{\circ}_{m,\,sPP}$ and $T^{\circ}_{m,\,PEP}$ as a function of wt_{PEP}, which are determined from DSC measurements and will be discussed later. It should be noted that the interaction parameter χ, based on the Flory–Huggins theory, originally only accounts for the enthalpic contribution and has the form b/T, with a positive constant b. As such, the Flory–Huggins theory predicts only the UCST phase separation. However, most experiments have shown that the Flory–Huggins theory still predicts the LCST phase behavior very well, with χ having the form of $a + b/T + c$, with negative b.[26,27]

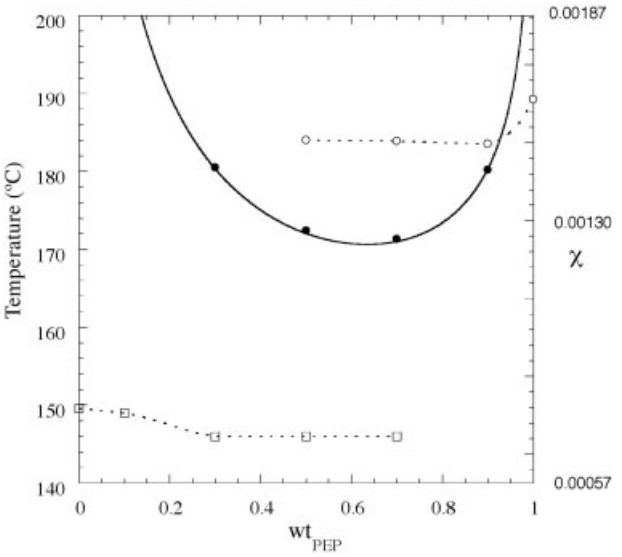

Figure 3. Calculated phase diagram of the sPP/PEP blends in terms of χ and wt_{PEP} for $N_{sPP,w} = 3024$ and $N_{PEP,w} = 1008$. The circles correspond to the measured L–L coexistence temperatures determined by cloud point measurements (CPM). The open circles and open squares correspond to the equilibrium melting temperatures of PEP and sPP, respectively, determined by DSC measurements for the blends first melted at 200 °C for 10 min and then isothermally crystallized at various temperatures.

Crystallization Behavior

Figure 4(a) shows the DSC heating scans of pure sPP that is isothermally crystallized at various values of T_c and then heated at a rate of 4 °C/min. It is evident that two melting temperature peaks for the sPP component, $T_{m1,sPP}$ and $T_{m2,sPP}$, as indicated by arrows in Figure 4(a), are observed when $T_c < 100$ °C. When $T_c > 100$ °C, the higher melting temperature peak $T_{m2,sPP}$ disappears. It should be noted that $T_{m2,sPP}$ also disappears with an increase in the heating rate. As T_c increases, both $T_{m1,sPP}$ and $T_{m2,sPP}$ exhibit a linear relationship with T_c. By extrapolating both lines of $T_{m1,sPP}$ versus T_c and $T_{m2,sPP}$ versus T_c to the line $T_m = T_c$, according to the linear Hoffman–Weeks analysis,[28] we obtain the same value of the equilibrium melting temperature of sPP, $T^{\circ}_{m,sPP}$, which is around 150 °C. These results suggest that only one unit-cell structure of sPP crystals that has been identified as an orthorhombic system by wide-angle X-ray diffraction (WAXD),[29] forms during the crystallization process. The low temperature melting peak ($T_{m1,sPP}$) is a result of the melting of the primary crystallites formed during the isothermal crystallization process, while the occurrence of the high melting temperature peak $T_{m2,sPP}$ refers to the melting of the crystallites recrystallized during the heating process. Our results are in good agreement with Supaphol,[30] in which the origin of the multiple melting behavior of sPP was explained in detail.

Figure 4(b) shows the DSC melting endotherms of pure PEP isothermally crystallized at various values of T_c, with a heating rate of 4 °C/min. Three

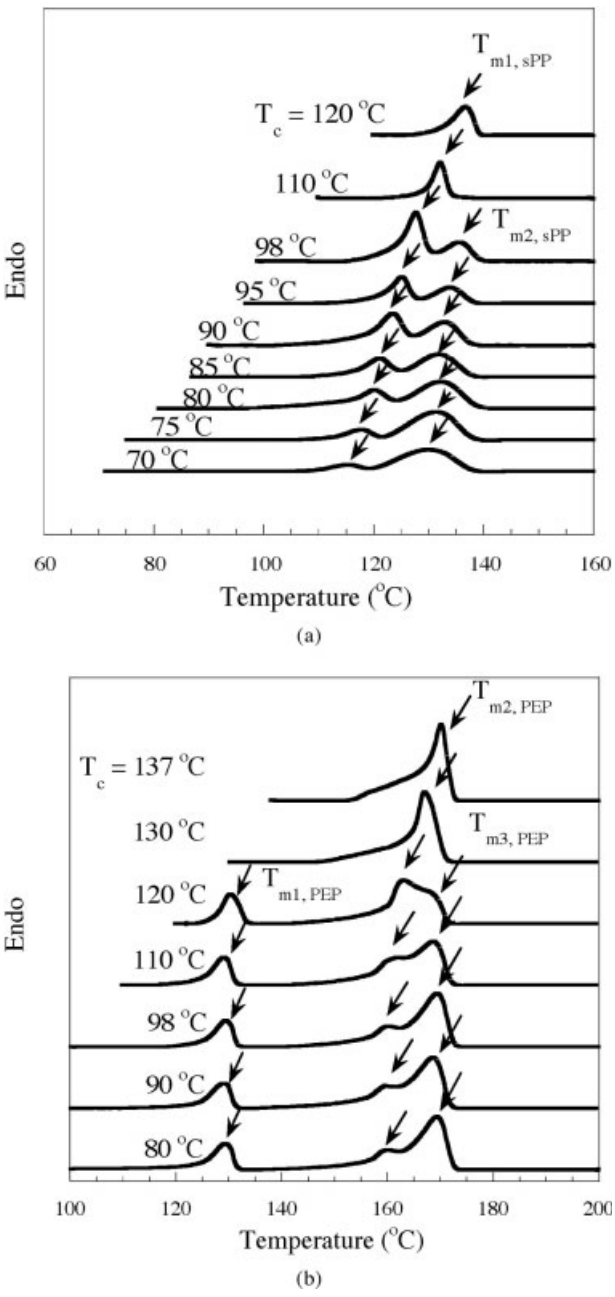

Figure 4. DSC melting endotherms of (a) pure sPP and (b) pure PEP after isothermal crystallization at various temperatures with a heating rate of 4 °C/min.

distinct melting temperature peaks for the PEP component, $T_{m1,PEP}$, $T_{m2,PEP}$, and $T_{m3,PEP}$, are observed when $T_c \leq 120$ °C. Moreover, both $T_{m1,\ PEP}$ and $T_{m3,PEP}$ are independent of T_c, and even disappear when T_c increases and is greater than 120 °C. $T_{m2,PEP}$ is observed to linearly increase with T_c, when $T_c \geq 120$ °C. According to the linear Hoffman–Weeks analysis, the equilibrium melting temperature of PEP, $T^{\circ}_{m,PEP}$, is found to be equal to 189 °C. Note that the three melting peak temperatures $T_{m1,PEP}$, $T_{m2,PEP}$, and $T_{m3,PEP}$, are always observed at low T_c values, with heating rates ranging from 4 °C/min to 50 °C/min. In addition, our WAXD analysis[29] indicates that PEP crystals belong to the monoclinic system. Therefore, we believe that the existence of $T_{m1,PEP}$, $T_{m2,PEP}$, and $T_{m3,PEP}$ corresponds to the melting of the three primary lamellar sizes of PEP crystallites formed during the isothermal crystallization process at low temperatures.

Similar to the analysis for sPP and PEP components, we employ DSC experiments for sPP/PEP blends, with wt_{PEP} varying from 0.1 to 0.9, first melted at 200 °C for 10 min and then isothermally crystallized at various values of T_c. As such, the equilibrium melting temperature of both sPP and PEP, $T^{\circ}_{m,sPP}$ and $T^{\circ}_{m,PEP}$, are analyzed as a function of wt_{PEP}. In general, the melting crystallization behaviors we obtain for pure sPP and PEP components are also preserved for each blend system we study here. For example, Figure 5 exhibits the DSC heating scans of sPP/PEP blends with various values of wt_{PEP} crystallized at T_c = 110 °C. In Figure 6(a,b) we present $T_{m1,sPP}$ versus T_c and $T_{m2,PEP}$ versus T_c, respectively, for sPP/PEP blends, from which the equilibrium melting temperatures $T^{\circ}_{m,sPP}$ and $T^{\circ}_{m,PEP}$ as a function of wt_{PEP} are determined and shown in Figure 3. We observe that $T^{\circ}_{m,PEP}$ for blends with wt_{PEP} ranging from 0.5 to 0.9 is almost the same but slightly smaller than that for pure PEP, and $T^{\circ}_{m,sPP}$ for wt_{PEP} = 0.3–0.7 is the same but slightly smaller than that for pure sPP. These results are not surprising because the sPP/PEP blends with wt_{PEP} = 0.3–0.9, initially melted at 200 °C, lie inside the two L–L phase region. The melting-point depression obtained for sPP and PEP components results from the PEP component dissolved in the sPP-rich domains, and sPP in the PEP-rich phase, respectively. Furthermore, the fact that both the $T^{\circ}_{m,sPP}$ and $T^{\circ}_{m,PEP}$ for the blends inside the two-phase region, after annealing at 200 °C for 10 min, are identical suggests that each phase domain has already reached the equilibrium concentration.

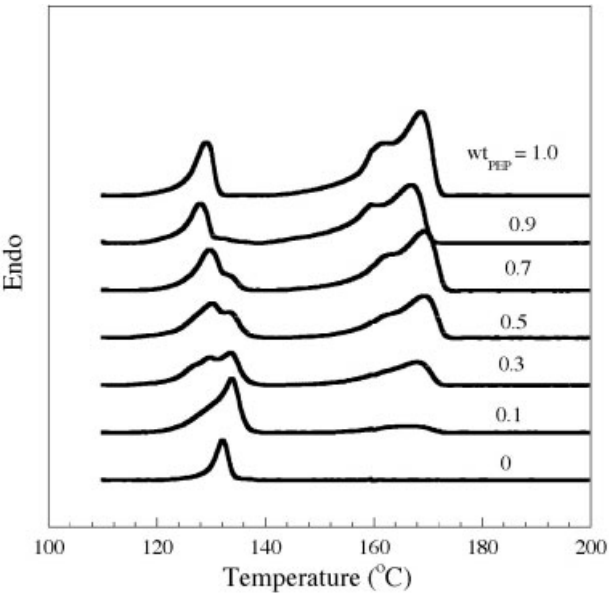

Figure 5. DSC heating scans of sPP/PEP blends with various values of wt_{PEP}, crystallized at T_c = 110 °C with a heating rate of 4 °C/min.

To determine the crystallinity of sPP and PEP in the blends, $X_{C,\ sPP}$ and $X_{C,\ PEP}$, the apparent enthalpy of melting per gram of blend ΔH^{*}_{blend}, obtained from the areas of the melting peaks of the DSC heating curves, must be divided into

$$\Delta H^{*}_{blend} = \Delta H^{*}_{blend,sPP} + \Delta H^{*}_{blend,PEP} \tag{3}$$

where $\Delta H^{*}_{blend,\ sPP}$ and $\Delta H^{*}_{blend,\ PEP}$ are the enthalpy per gram of blend contributed from the melting of sPP and PEP crystals. Then $X_{C,\ sPP}$ and $X_{C,\ PEP}$ in the blends can be determined by

$$X_{C,sPP} = \Delta H^{*}_{blend,sPP}/\Delta H^{\circ}_{sPP} \tag{4a}$$

$$X_{C,PEP} = \Delta H^{*}_{blend,PEP}/\Delta H^{\circ}_{PEP} \tag{4b}$$

where ΔH^{*}_{sPP} and ΔH^{*}_{PEP} are the heat of melting per gram of 100% crystalline sPP and PEP, and equal to 196.6 J/g[31] and 209 J/g,[32] respectively.

For the neat sPP and PEP polymers, the enthalpy of melting per gram for each crystallization temperature T_c is simply obtained by integrating the melting peaks of the DSC heating scans, as shown in Figure 4(a,b). Because the melting curves for the pure SPP and PEP components overlap at around 130 °C, for the sPP/PEP blends crystallized at a T_c below both melting temperatures, as shown in Figure 5, it is hard to separate ΔH^{*}_{blend} into $\Delta H^{*}_{blend,\ sPP}$ and $\Delta H^{*}_{blend,\ PEP}$

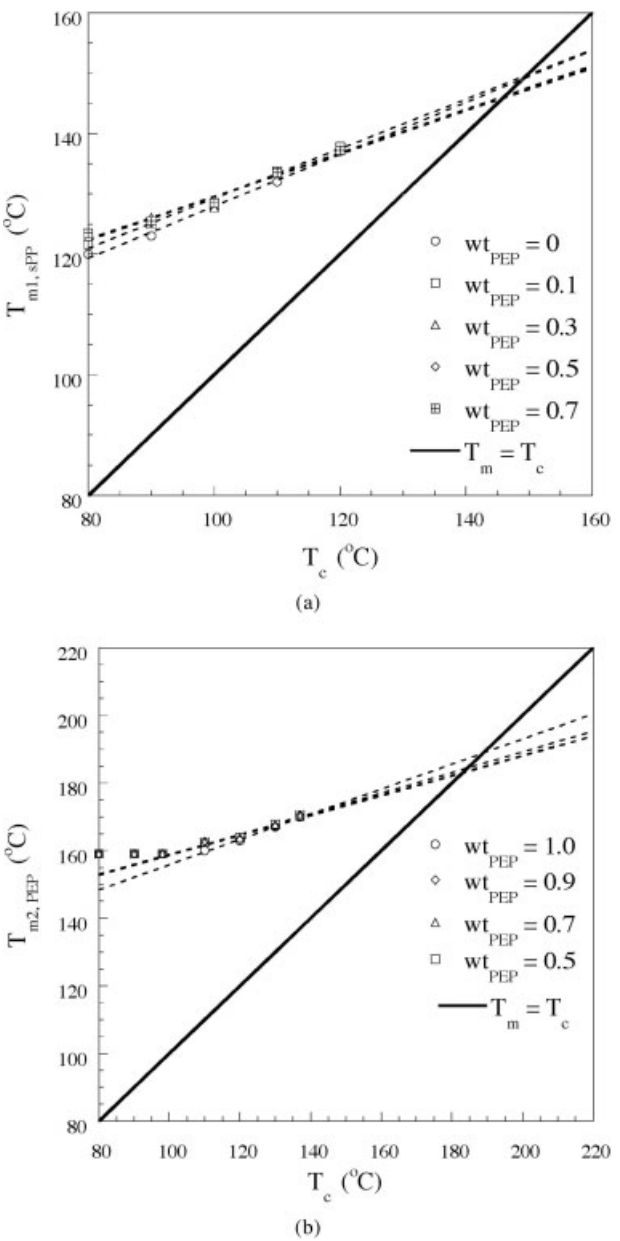

Figure 6. Variation of (a) $T_{m1,sPP}$ and (b) $T_{m2,PEP}$ with T_c for the sPP/PEP blends with various values of wt_{PEP}.

directly. The calculation of sPP and PEP crystallinities becomes more complicated. However, by deconvoluting the DSC profiles to a combination of possible melting peaks with Gaussian curves that originate from simulating the DSC heating scans of the neat sPP and PEP polymers, we can separate the melting peaks as well as the enthalpy of heating contributed from each component. As a result, the crystallinities of each component, $X_{C,\ sPP}$ and $X_{C,\ PEP}$, are determined by eq 3 and eq 4 and are listed in Table 1.

Table 1. Comparison of Experimental and Calculated Crystallinities of PEP and sPP for Various Values of wt_{PEP} and T_c

wt_{PEP}	T_c (°C)	$X_{C,\ PEP}$ (exp)	$X_{C,\ PEP}$ (cal)	$X_{C,\ sPP}$ (exp)	$X_{C,\ sPP}$ (cal)
1	137	0.2793			
	130	0.2736			
	120	0.3375			
	110	0.3606			
	98	0.3552			
	90	0.3704			
	80	0.3772			
0.9766	137		0.2745		0
	130		0.2643		0
	120		0.3296		0
	110		0.3522		0
	98		0.3556		0
	90		0.3618		0
	80		0.3732		0
0.9	137	0.2286	0.2495	0	0
	130	0.2461	0.243	0	0
	120	0.3065	0.3063	0.0049	0.0045
	110	0.3158	0.3271	0.0040	0.0052
	98	0.3274	0.3267	0.0128	0.0111
	90	0.3206	0.3327	0.0138	0.0114
	80	0.3492	0.3445	0.0072	0.0122
0.7	137	0.1767	0.1842	0	0
	130	0.1825	0.1874	0	0
	120	0.2382	0.2456	0.0223	0.0163
	110	0.2564	0.2618	0.0211	0.0188
	98	0.2517	0.2512	0.0439	0.0400
	90	0.2520	0.2569	0.0368	0.0411
	80	0.2662	0.2697	0.0350	0.0441
0.5	137	0.1311	0.1189	0	0
	130	0.1316	0.1318	0	0
	120	0.1850	0.1848	0.0303	0.0280
	110	0.1936	0.1964	0.0369	0.0324
	98	0.1753	0.1756	0.0602	0.0688
	90	0.1751	0.1810	0.0675	0.0709
	80	0.1979	0.1949	0.0767	0.0760
0.3	137	0.0277	0.0536	0	0
	130	0.0740	0.0762	0	0
	120	0.1178	0.1240	0.0349	0.0397
	110	0.1242	0.1311	0.0463	0.0461
	98	0.1015	0.1001	0.0969	0.0977
	90	0.1013	0.1052	0.0937	0.1006
	80	0.1139	0.1200	0.1175	0.1079
0.1375	137		0.0006		0
	130		0.0311		0
	120		0.0747		0.0493
	110		0.0780		0.0571
	98		0.0388		0.1212
	90		0.0436		0.1248
	80		0.0592		0.1339
0.1	137	0.0006		0	
	130	0.0077		0	
	120	0.0357		0.0509	
	110	0.0474		0.0600	
	98	0.0296		0.1207	
	90	0.0378		0.1198	
	80	0.0430		0.1341	
0	120			0.0494	
	110			0.0550	
	98			0.1286	
	90			0.1439	
	80			0.1552	

It is interesting to note that for blends initially undergoing L–L phase separation into sPP-rich and PEP-rich domains in the molten state, such as wt_{PEP} in the range of 0.3–0.9 at 200 °C for 10 min, the values of $X_{C,sPP}$ and $X_{C,PEP}$ obtained from analyzing the DSC heating profiles after they are isothermally crystallized at T_c satisfy the following equations:

$$X_{C,sPP} = \nu^{\alpha} X^{\alpha}_{C,sPP} + \nu^{\beta} X^{\beta}_{C,sPP}$$

$$X_{C,PEP} = \nu^{\alpha} X^{\alpha}_{C,PEP} + \nu^{\beta} X^{\beta}_{C,PEP} \quad (5)$$

where α and β denote the coexisting sPP-rich and PEP-rich phase, respectively, and $X^{\alpha}_{C,\,I}$ and $X^{\beta}_{C,\,I}$ are the crystallinity of component I (I = sPP, PEP) in the α and β phases. The volume fractions of α and β, denoted as ν^{α} and ν^{β}, respectively, are determined by

$$\nu^{\alpha} = \frac{\phi^{\beta}_{PEP} - \phi_{PEP}}{\phi^{\beta}_{PEP} - \phi^{\alpha}_{PEP}}$$

$$\nu^{\beta} = 1 - \nu^{\alpha} \quad (6)$$

where ϕ^{α}_{PEP} and ϕ^{β}_{PEP} correspond to the volume fraction of PEP in the α and β phase, respectively, and can be determined by our previous thermodynamic analysis, according to Flory–Huggins theory. For example, ϕ^{α}_{PEP} and ϕ^{β}_{PEP} are equal to 0.1375 and 0.9766, respectively, at 200 °C. The values of ν^{α} and ν^{β} for each system with a known ϕ_{PEP} are then calculated with eq 6. As can clearly be seen in eq 5, the crystallinity of each component I (I = sPP, PEP) in α and β, $X^{\alpha}_{C,\,I}$ and $X^{\beta}_{C,\,I}$, can be solved by inserting the experimental values of $X_{C,\,sPP}$ and $X_{C,\,PEP}$ for any two systems with wt_{PEP} between 0.3 and 0.9, and then averaged, as summarized in Table 1. With these average values, $X^{\alpha}_{C,\,I}$ and $X^{\beta}_{C,\,I}$, we obtain the calculated values of $X_{C,\,sPP}$ and $X_{C,\,PEP}$ for a given ϕ_{PEP} by eq 5, and compare them with the experimental results in Table 1. Clearly, both calculated and experimental results are in good agreement. These results again manifest the fact that our previous thermodynamic analysis with Flory–Huggins theory describes the LCST phase behavior of sPP/PEP blends very well. Furthermore, each separated domain for the blends inside the two-phase region, after annealing at 200 °C for 10 min, reaches the equilibrium concentration as well as the phase volume fraction predicted by Flory–Huggins analysis.

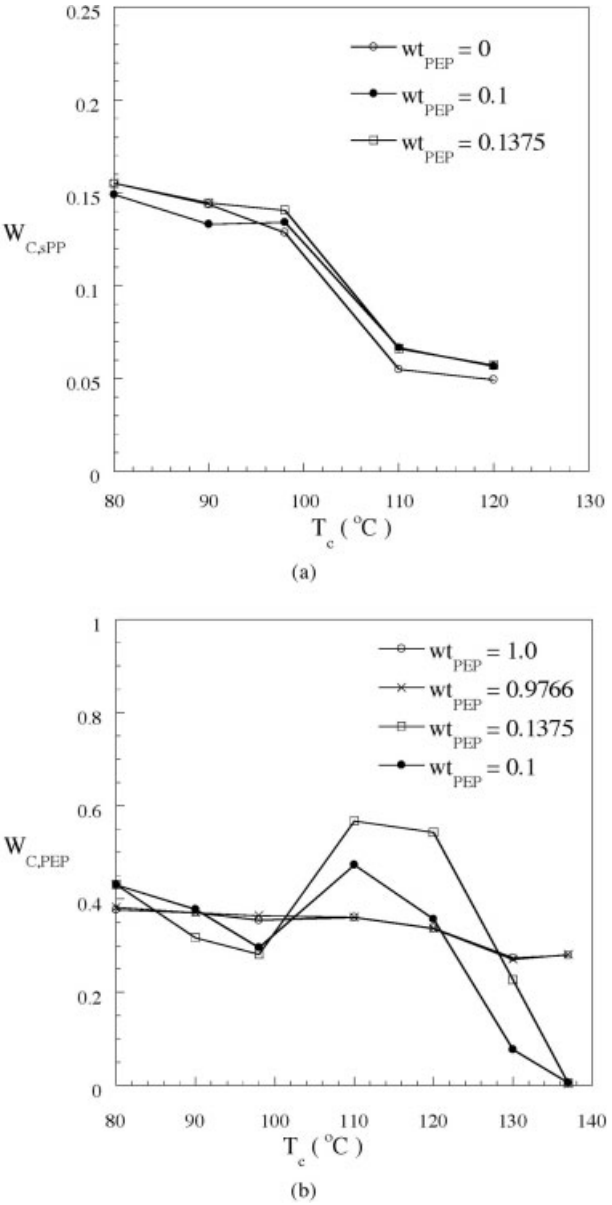

Figure 7. Plot of the normalized crystallinity of (a) sPP component, $W_{C,\,sPP}$, and (b) PEP component, $W_{C,PEP}$, as a function of T_c for systems with various values of wt_{PEP} initially occurring in the one homogeneous phase region when melted at 200 °C for 10 min.

To examine the effects of blending on the crystallizability of PEP and sPP, we plot the normalized crystallinity of PEP and sPP, defined as

$$W_{C,sPP} = X_{C,sPP}/(1 - wt_{PEP})$$

$$W_{C,PEP} = X_{C,PEP}/wt_{PEP} \quad (7)$$

for the blends that are initially in the one-phase region in Figure 7(a,b). We observe that the nor-

malized sPP crystallinity is almost the same for sPP-rich blends, such as wt_{PEP} = 0, 0.1, and 0.1375, which indicates that the crystallizability of sPP is not influenced by the presence of a small amount of PEP. Similar behavior for PEP crystallization in the PEP-rich blends is also observed, as shown in Figure 7(b). However, for sPP-rich systems, such as wt_{PEP} = 0.1 and 0.13746, we find that the minority PEP still can crystallize, and the normalized PEP crystallinity is seen to be greater than that for pure PEP when T_c is around 110–120 °C; it drops dramatically to 0 as $T_c > 120$ °C. A reasonable explanation may be given as follows. Because the process of crystallization for blends is nucleation and growth with nucleation being most often heterogeneous,[33] it seems likely that the PEP nucleation density increases with an increase in the amount of sPP. However, upon blending with more sPP, the PEP molecular mobility in the sPP-rich domains decreases. When the T_c is high (e.g., > 120 °C) because the decreasing degree of the PEP mobility is much larger than the increasing degree of the formed nuclei, the crystallizability of PEP is depressed significantly. As the T_c decreases (e.g., in the range of 110–120 °C), because of the great increase of the nucleation density which even overcomes the reduction of the mobility, we observe that the crystallization of PEP greatly increases. However, with a further decrease in the T_c, although the formed nucleation density increases, it is balanced with the mobility reduction, and the normalized PEP crystallinity in the sPP-rich blends is almost the same as that for pure PEP.

CONCLUSIONS

We employ phase-contrast microscopy (PCM), cloud point measurement (CPM), and differential scanning calorimetry (DSC) to study the L–L phase separation behavior as well as the crystallization behavior in crystalline blends of sPP and PEP. In particular, the effects of L–L spinodal decomposition on the crystallization of both sPP and PEP components are analyzed.

The time-evolved PCM micrographs for the sPP/PEP blends annealed above the melting temperatures of sPP and PEP clearly show the bicontinuous interconnected structures resulting from the L–L phase separation. As the separation temperature increases, the characteristic phase domain size increases with the temperature. This indicates that blends of sPP and PEP exhibit a LCST phase behavior in the melt. The L–L phase diagram, constructed in terms of temperature and wt_{PEP} by CPM, is well described by the theoretical prediction based on the Flory–Huggins free energy functional with $\chi(T) = 0.01153 - 4.5738/T(\mathrm{K})$.

From the DSC melting endotherms, the melting temperatures and the crystallinities of both sPP and PEP components are analyzed as a function of wt_{PEP} and T_c. The equilibrium melting temperature of each component is then determined according to the linear Hoffman–Weeks extrapolations. For the sPP/PEP blends that are crystallized from two segregated sPP-rich and PEP-rich phases in the melt, because of the fact that each phase domain reaches the equilibrium concentration ϕ^{α}_{PEP} and ϕ^{β}_{PEP} as well as the phase volume fraction ν^{α} and ν^{β} determined by the LCST coexistence curve, the equilibrium melting temperature of each component in the blends remains a constant that is slightly lower than that for the neat polymer. The crystallinity of each component also follows the equation: $X_{C,I} = \nu^{\alpha} X^{\alpha}_{C,I} + \nu^{\beta} X^{\beta}_{C,I}$, I = PEP, sPP. For the sPP/PEP blends crystallized from one homogeneous phase in the melt, the presence of only a small amount of the minority component has almost no influence on the crystallizability of the major component. However, the crystallizability of the minority component is greatly affected by the presence of the major component. One may expect that the molecular mobility of the minority component is retarded, but the heterogeneous nucleation density is promoted upon blending with a majority. Therefore, the significant reduction of the minority crystallizability when the T_c is high is mainly because of the decrease of the minority mobility that is hindered by the presence of the major component. The increase of the minority crystallizability in the intermediate region of the T_c is mainly because of the great increase of the heterogeneous nuclei upon blending with a major component.

The authors gratefully acknowledge support from the National Science Council of the Republic of China through grant NSC 91-2216-E-011-024.

REFERENCES AND NOTES

1. Martuscelli, E.; Silvestre, C.; Gismondi, C. Makromol Chem 1985, 186, 2161.
2. Lohse, D. J Polym Eng Sci 1986, 26, 1500.
3. (a) Hashimoto, T.; Inaba, N.; Sato, K; Suzuki, S. Macromolecules 1986, 19, 1690; (b) Hashimoto, T.; Inaba, N.; Yamada, T; Suzuki, S Macromolecules 1988, 21, 407.

4. Ito, H.; Russell, T. P.; Wignall, G. D. Macromolecules 1987, 20, 2213.
5. Martuscelli, E.; Vicini, L.; Seves, A. Makromol Chem 1987, 188, 607.
6. Burghardt, W. R. Macromolecules 1989, 22, 2482.
7. Addonozio, M. L.; Martuscelli, E.; Silvestre, C. J Polym Mater 1990, 7, 63.
8. (a) D'Orazio, L.; Mancarella, C.; Martuscelli, E.; Sticotti, G. J Mater Sci 1991, 26, 4033; (b) D'Orazio, L.; Mancarella, C.; Martuscelli, E.; Sticotti, G.; Massari, P. Polymer 1993, 34, 3671; (c) D'Orazio, L.; Mancarella, C.; Martuscelli, E.; Sticotti, G.; Ghisellini, R. J Appl Polym Sci 1994, 53, 387.
9. Nojima, S.; Sato, K.; Ashida, T. Macromolecules 1991, 24, 942.
10. Tomura, H.; Sato, H.; Inoue, T. Macromolecules 1992, 25, 1611.
11. Cham, P. M.; Lee, T. H.; Marand, H. Macromolecules 1994, 27, 4263.
12. Chen, H. L. Macromolecules 1995, 28, 2845.
13. Chen, C. Y.; Yunus, W. Md. Z. W.; Chiu, H. W.; Kyu, T. Polymer 1997, 38, 4433.
14. D'Orazio, L.; Mancarella, C.; Martuscelli, E.; Sticotti, G.; Cecchin, G. J Appl Polym Sci 1999, 72, 701.
15. Lim, S. W.; Lee, K. H.; Lee, C. H., Polymer 1999, 40, 2837.
16. Ramanujam, A.; Kim, K. J.; Kyu, T. Polymer 2000, 41, 5375.
17. Lee, J. K.; Lee, J. H.; Lee, K. H.; Jin, B. S. J Appl Polym Sci 2001, 81, 695.
18. (a) Wang, H.; Shimizu, K.; Hobbie, E. K.; Wang, Z. G.; Meredith, J. C.; Karim, A.; Amis, E. J.; Hsiao, B. S.; Hsieh, E. T.; Han, C. C. Macromolecules 2002, 35, 1072; (b) Wang, H.; Shimizu, K.; Kim, H.; Hobbie, E. K.; Wang, Z. G.; Han, C. C. J Chem Phys 2002, 116, 7311.
19. Cheung, Y. W.; Stein, R. S. Macromolecules 1994, 27, 2512.
20. Cheung, Y. W.; Stein, R. S.; Lin, J. S.; Wignall, G. D. Macromolecules 1994, 27, 2520.
21. Thomann, R.; Kressler, J.; Setz, S.; Wang, C.; Mulhaupt, R. Polymer 1996, 37, 2627.
22. Thomann, R.; Kressler, J.; Rudolf, B.; Mulhaupt, R. Polymer 1996, 37, 2635.
23. Phillips, R. A. J Polym Sci Part B: Polym Phys 2000, 38, 1947.
24. Flory, P. J. In Principles of Polymer Chemistry; Cornell University Press: Ithaca, NY, 1953, p 495.
25. Brandrup, J.; Immergut, E. H.; Grulke, E. A. In Polymer Handbook; Wiley: New York, 1999, p v/24.
26. Roe, R. J.; Zin, W. C. Macromolecules 1980, 13, 1221.
27. Maruta, J.; Ougizawa, T.; Inoue, T. Polymer 1988, 29, 2056.
28. Hoffman, J. D.; Weeks, J. J Res Natl Bur Stand A 1962, 66, 13.
29. Huang, C. I.; Chen, J. R.; Wang, Z. G.; Hsiao, B. J. Macromolecules, to be submitted.
30. Supaphol, P. J Appl Polym Sci 2001, 82, 1083.
31. Hatka, S.; Konnecke, K. J Macromol Sci Phys1991, 30, 319.
32. Antberg, M.; Dolle, V.; Hattka, S.; Rohrmann, J.; Spaleck, W.; Winter, A.; Zimmermann, H. Macromol Chem Macromol Symp 1989, 30, 428.
33. Stein, R. S. Mater Res Soc Symp Proc 1994, 321, 531.